This is the Pre-Published Version.
Q. Xie, M. Gao, X. Huang (2020) *Fire Risk and Behavior of Rice during the Convective Drying Process*, **Fire Safety Journal** https://doi.org/10.1016/j.firesaf.2020.103013

Fire Risk and Behavior of Rice during the Convective Drying Process

Qiyuan Xie[1,*], Meng Gao[1], Xinyan Huang[2,*]

[1]State Key Lab of Fire Science, University of Science and Technology of China, Hefei 230027, China

[2]Department of Building Services Engineering, The Hong Kong Polytechnic University, Hong Kong, China

Abstract:

Drying of grain is a crucial process for long-term preservation, while having a significant fire risk. This work investigated the ignition risk and fire behavior of paddy rice (~1 kg) with the drying airflow velocity up to 0.9 m/s. Results showed that there was a minimum internal flow velocity for a given spotting ignition protocol, so that a stronger drying flow has a greater ignition risk. Once ignited, three stages of fire spread processes hidden below the surface were revealed, (I) smoldering spread, (II) flame spread, and (III) smoldering spread. The smoldering rice was glowing hot (800-900 °C). With a forced airflow, the downward smoldering spread (about 2 mm/min) was comparable to or faster than the horizontal spread, different from the natural smoldering fire. The regression of rice bed in Stage-I smoldering increased the drying airflow, which created a cavity and further accelerated the downward smoldering spread. Moreover, the smoldering-to-flaming transition is triggered to sustain the flame spread on and below the free surface. By increasing the drying flow velocity, the fire-spread rate, and the fire hazards in all stages increased. This work reveals the complex fire dynamics of rice storage and supports fire protection during the grain drying process.

Keywords: grain fire safety; paddy; ignition; fire spread; smoldering; drying airflow

1. Introduction

Rice is the staple food for more than half of the world's population, especially in Asian countries [1]. China is the world's largest rice producer and consumer, with rice production accounting for about 37% of the global production [2]. Therefore, the fire safety of rice during the processing, storage, and transportation becomes a critical concern. The typical paddy rice consists of white rice, bran, germ, and rice husk. The main components of white rice are fat, protein, and cellulose. Thus, rice is combustible in nature, and the rice husk is also widely used as biomass fuel [3-5]. A scientific understanding of the rice combustion characteristics is critical for assessing the fire risk of granaries and designing a more effective fire protection system. Most research efforts on the fire hazards of grain products and fuels have focused on the heat generation of grain, the risk of self-ignition, and the explosion of grain flour [6-9], but ignored their actual fire risk and behaviors of rice and other grains, especially during their complex industrial processes.

The water in rice storage creates a proper environmental condition to breed insects and bacteria [10]. The excessive moisture content of rice will not only increase the mildewing possibility and reduce the economic value of rice [11, 12] but also facilitate the self-heating in low temperature via exothermic biodegradation. Therefore, after harvest, the rice must be dried below 12~14% for minimizing the biodegradation processes caused by bacteria. There are various methods for drying grain, and the convective drying is most widely used, which can be classified by the direction of inner airflow through the grain, namely, cross-flow, counter-flow, and concurrent-flow drying processes [13-15]. The principle of these drying processes is to reduce the moisture by intense convective heat and mass transfer between the porous rice bed and internal airflow [16]. It is worth noting that the high-temperature process of drying has the most significant fire risk among all post-harvest processes. Comparatively, the fire risk in grain transportation and storage is much lower [17, 18], due to a scientific understanding of the self-heating ignition process (such as the critical storage size and self-ignition ambient temperature) [19], as well as a sophisticated fire protection regulation [20]. So far, many fire accidents have occurred in grain drying towers. For example, there was a fire accident in the tower in the Cenex Harvest States at Crookston, MN, USA, in 2009, where several re-ignition of flame occurred during the firefighting process [21]. More recently, fire events in the drying tower of a granary at Mount Pleasant, USA in 2018 [22] and at Melfort, Canada in 2019 [23] (Fig. 1), which might be caused by the self-ignition process.

* Corresponding authors: Qiyuan Xie (xqy@ustc.edu.cn) and Xinyan Huang (xy.huang@polyu.edu.hk)

Fig. 1 Recent fire accidents in rice storage and drying processing at (a) Crookston, MN, USA in 2019 [21], (b) Mount Pleasant, USA in 2018 [22], and (c) Melfort, Canada in 2019 [23].

There are two major reasons for the significant fire risk during the convective drying process of rice, (1) the heating components or the hot burning fuels, which are used to heat the airflow, may accidentally enter the drying equipment [13, 24] and cause the spotting ignition of a fire[1] [25, 26], and (2) the high-temperature drying airflow in the equipment enhances the heterogeneous oxidation inside the porous grain [27]. Like most natural biomasses, such as wood, peat, and coal [26-29], rice and other grains can support both smoldering and flaming fires. Smoldering is a slow, low-temperature, flameless, and most persistent type of combustion [30], which plays a central role in the self-heating ignition. Flaming fire is more intense, has a faster heat release rate, and can spread at least two orders of magnitude faster than smoldering, but a stronger ignition source is required to initiate a flame. Nevertheless, flaming fire and smoldering fire can easily transition to each other under proper environmental conditions [31, 32]. In order to evaluate the fire risk and hazard of rice and other grain during the drying process, it is essential to gain a more scientific understanding of different combustion and fire characteristics of these grain fuels under the convective drying airflow.

In this work, we designed an experimental platform to study the ignition risk of rice under different drying airflows, and the combustion characteristics of rice after ignition. The fire dynamics and the influence of airflow velocity on ignition and fire spread were analyzed to help develop fire-protection strategies during the grain drying process.

2. Experimental methods

Figure 2 shows the schematic diagram of the experimental setup that simulates the industrial drying process of rice and the fire scenario initiated by a spotting ignition. The cylindrical drying chamber for rice had a volume of 2.1 L with a diameter of 21 cm and a depth of 6 cm, which was a 1/10 reduced scale model of the industrial drier and provided by the industrial collaborator. It was made of stainless steel and covered by a 5-mm thick layer of the thermal-insulation fiberglass. The rice bed was held by a porous metal mesh plate, and an electronic balance was placed at the bottom to measure the mass loss of rice during the burning process. Below the drying section, there was the conical flow duct. An extraction fan was connected in the outlet to produce a forced airflow that penetrates the rice sample from the top free surface. The velocity of drying airflow could be adjusted by varying the power of the fan.

For each experiment, about 1150 g of paddy rice sample (i.e., with the outer husk) was filled into the drying chamber. Thus, the bulk density of paddy rice was 550 kg/m^3. Considering the solid density of 1200 kg/m^3 [33], the porosity of paddy (ϕ) was 0.58. The thermogravimetric analysis (TGA) was conducted for this rice sample (see Fig. A1 in the Appendix). To determine the original moisture content of rice, the rice was drying in an oven at 105 ℃ for 10 h. Then, the mass-based moisture content (MC) of rice sample is

$$MC = \frac{m_w - m_{dr}}{m_{dr}} \times 100\% = 14 \pm 2\% \qquad (1)$$

where m_w and m_{dr} are the mass of the rice before and after drying, respectively.

[1] The spot fire ignition is caused by hot (solid, molten oxidizing or burning) metal fragments/sparks and firebrands (flaming or glowing embers), which is an important fire ignition pathway industrial and wildland fire.

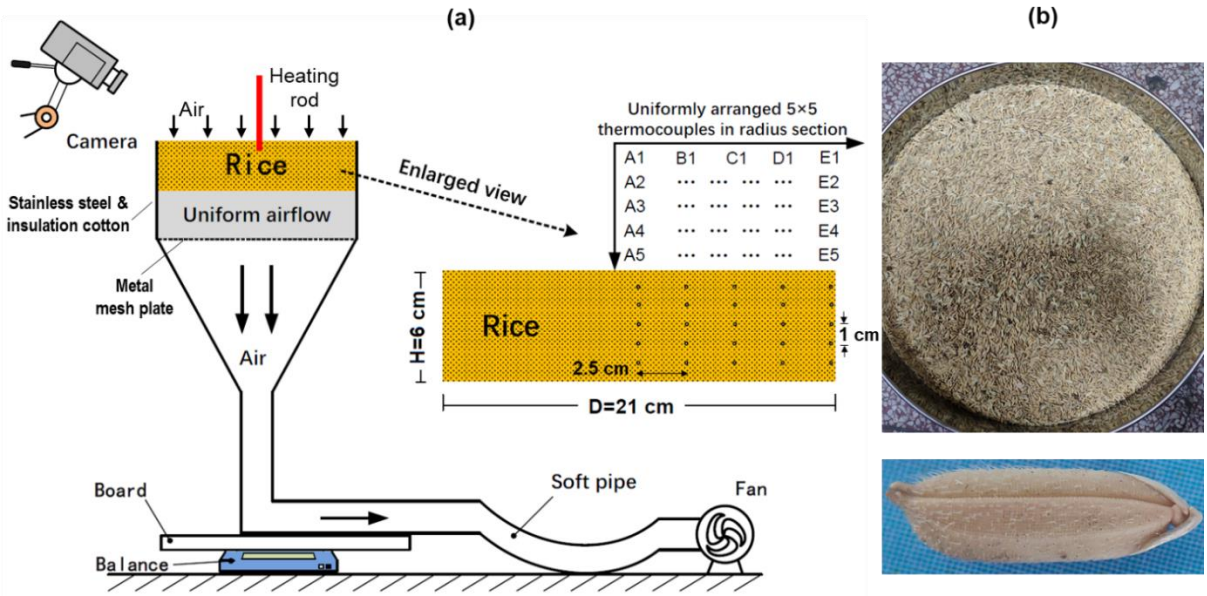

Fig. 2. (a) Schematics of the rice drying chamber with a downward airflow, and (b) photo of rice sample and particle.

Inside the rice bed, there was a matrix (5×5) of thermocouples, evenly inserted from one side of the chamber to its central plane. These armed K-type thermocouples had a bead diameter of 1 mm. The thermocouple matrix had a vertical spacing of 1 cm and a horizontal spacing of 2.5 cm, where column A roughly overlapped with the central axis. Thermocouple wires and flow pipes were not stretched when connecting to the combustion chamber, which limited the interference of fan vibration and wiring tension on the measurement of mass loss. An electric rod igniter was used to mimic the potential spotting ignition by hot metal particles or burning fuels. The igniter had a diameter of 1cm, a length of 8 cm, a default power of 200 W, and a surface temperature of about 800 °C. Only the tip of igniter was inserted into the rice sample with a depth of 1 cm, which created a hot spot, so that the effective ignition power was about 15% default power. For all tests, the ignition duration was fixed to be 10 min, and the drying airflow was on during the ignition.

By controlling the fan in Fig. 2, the ignition and fire experiments were conducted for the rice stack with a drying airflow in the downward direction. Throughout all tests, the airflow was not heated, so its temperature was the same as the room temperature of 27±2 °C. The airflow velocity inside the porous rice bed (U_a) was calculated based on the volumetric flow rate ($\dot{Q}$), the cross-section area of the drying chamber (A), and the porosity of rice bed (ϕ) as

$$U_a = \frac{\dot{Q}}{\phi A} \tag{2}$$

Six different velocities of such internal airflow were tested, i.e., 0 m/s (no forced flow), 0.2 m/s, 0.4 m/s, 0.6 m/s, 0.8 m/s and 0.9 m/s, respectively, which were also typically used in the industrial application. Note that without the forced flow, there would still be diffusion and natural convection to feed oxygen for the burning of rice. A high-definition digital camera was placed above the combustion chamber to monitor the ignition and development of rice burning processes. At least two experiments were conducted for each test condition. If there were large variations of test outcomes, especially near the limiting condition, more repeating tests were conducted to ensure good experimental repeatability.

3. Results and discussion

3.1. Ignition of rice

Figure 3 shows the outcome of the entire ignition and burning of rice under six different airflow velocities from 0 to 0.9 m/s. The original test videos can be found in the *Supplemental Materials* (Videos S1-4 with 50 times playback speed). Figure 4 shows the corresponding curves of mass loss and the mass-loss rate. Clearly, there is a minimum internal airflow velocity under the given ignition protocol of about 0.6 m/s. As the airflow velocity was increased, the oxygen supply became abundant in the rice stack, thus promoting the heterogeneous oxidation (or smoldering combustion) during the ignition process [27]. When the airflow was below 0.6 m/s, only the rice near the igniter was charred (see Fig. 3a-c and Video S1), while a self-sustained

smoldering front could not be produced under the limited ignition duration. In other words, the ignition and fire risks of rice are greater under a larger drying airflow.

During the 10-min ignition, a stable flame could be observed near the ignitor. The thermocouple near the ignitor gradually increased and eventually exceeded 800 °C, which was much higher than the threshold temperatures of pyrolysis (300 °C) and char oxidation (400 °C) in Fig. A1. Both the existence of flame on the sample surface and the thermocouple measurements inside the rice bed have demonstrated that the ignition process was robust. After turning off the igniter, the flame could no longer be sustained on the rice surface.

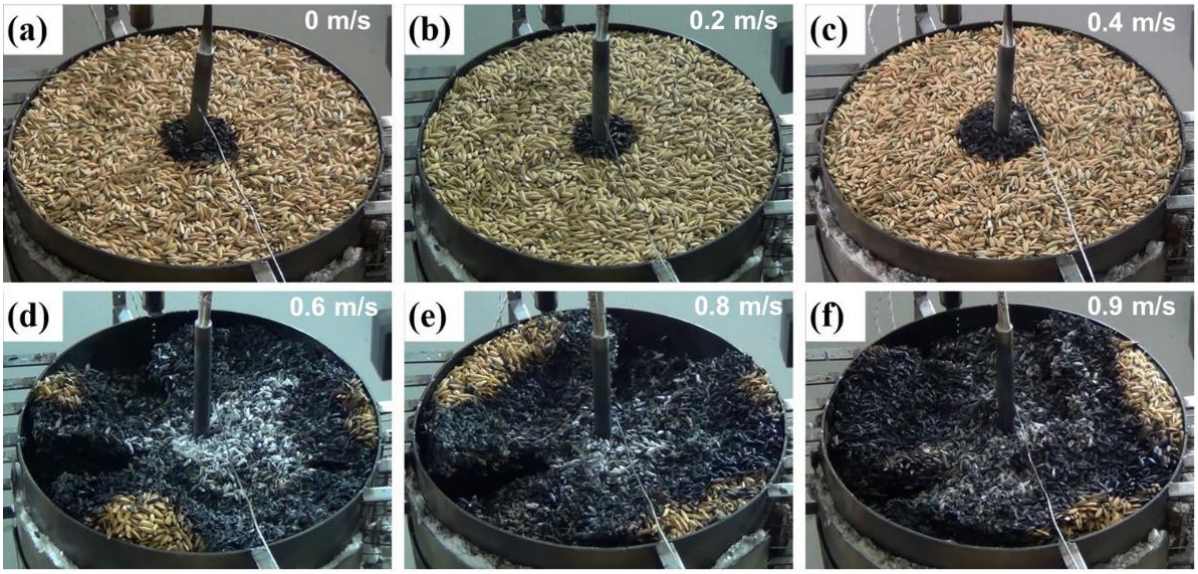

Fig. 3. The outcomes and residues of ignition and burning of rice under drying airflow velocities of (a) 0 m/s without airflow, (b) 0.2 m/s, (c) 0.4 m/s (Video S1), (d) 0.6 m/s (Video S2), (e) 0.8 m/s (Video S3), and (f) 0.9 m/s (Video S4).

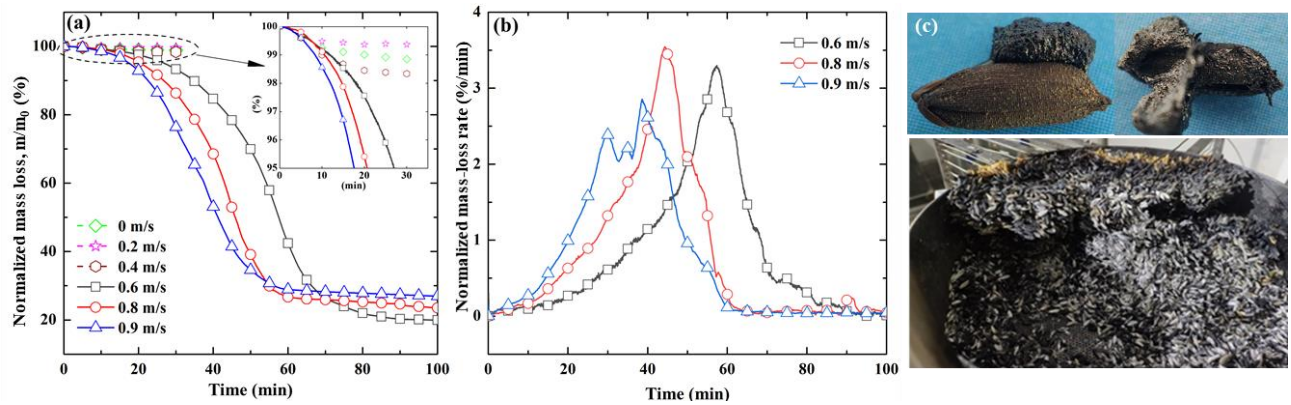

Fig. 4. (a) Normalized mass loss and (b) mass-loss rate under different internal drying airflow velocities ranging from 0 to 0.9 m/s, where the original mass of rice sample is about 1150 g, and (c) the burning residue of rice particle and bed.

The mass loss during ignition was less than 20 g or less than 2% of the original mass, as shown in Fig. 4a. On the other hand, once ignited, about 80% of the rice bed was burnout, except for some quenched near the cold metal wall and the bottom of the dry chamber [34] (see Fig. 3d-f). Once heated, the rice particle would first thermally expand, melt, and then breach the outer husk. Afterward, the hot molten rice flowed out and was pyrolyzed to release pyrolysis gas and form char and tar, as shown in Fig. 4c.

Moreover, the larger the airflow velocity, the earlier the peak of mass-loss rate appears (Fig. 4b), which indicates a faster development and spread of fire and an increase of the fire heat release rate (HRR). The reason is that the early-stage burning of rice was dominated by the form of smoldering combustion, which is controlled by the oxygen supply [35, 36]. Therefore, as the larger airflow brought more oxygen, the burning rate became faster and reached a peak earlier. Note that as the burning of the rice sample continued, the internal airflow velocity would increase due to the decrease in flow resistance. Therefore, near burnout, the airflow velocity was much larger, which also enhanced convective cooling effect and quenching near the chamber wall, resulting in a slightly more residue for a larger airflow velocity.

3.2. Fire development on rice

Figure 5 shows a series of photos for ignition and fire development processes on the rice bed with a forced drying airflow of 0.6 m/s (also see Video S2). As most of the fire processes were hidden below the charred top surface, Figure 6 shows the corresponding thermocouple temperature measurements inside the rice bed, which were reconstructed into a temperature contour in Fig 7a and Video S5 to illustrate the internal fire spread process. Figure 8 shows a diagram that summarizes the three-stage fire-spread process on the rice bed.

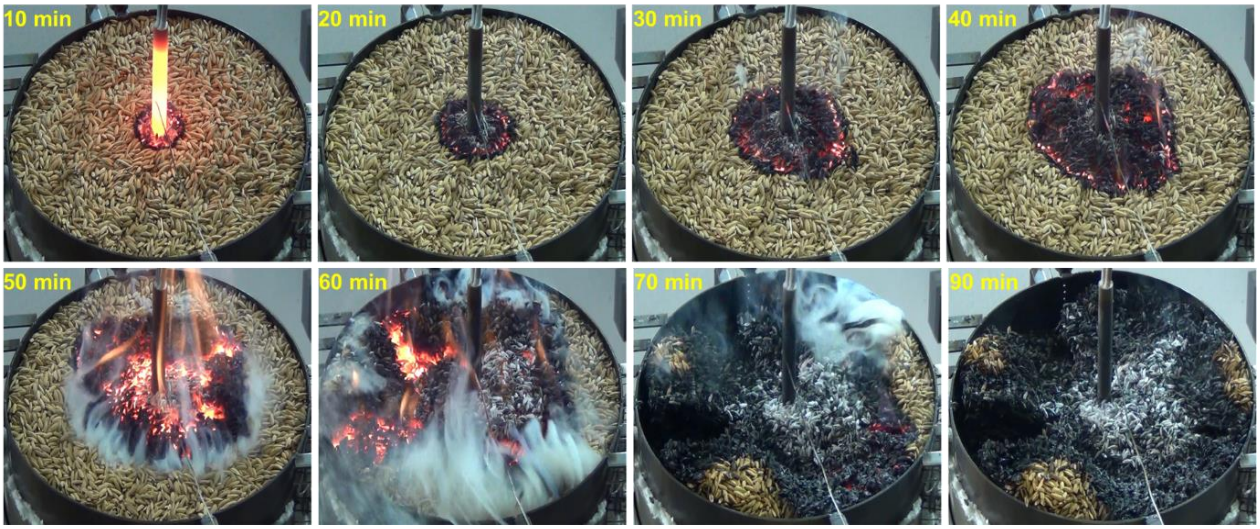

Fig. 5. Photos of rice ignition and combustion experiment with the downward drying airflow of 0.6 m/s (Video S2).

Stage-I Smoldering Spread. After turning off the hot ignition rod, a charred black ring was formed around the rod. The top-view camera also captured a glowing red edge that was formed in the outer perimeter, that is, the smoldering fire front. Along with the continuous smoldering spread process, the charring (smoldering) region expanded steadily and uniformly on the top free surface within the first 30 min. Note that small flames were also observed in the fire inception, which was the ignited rice husk, rather than the rice particle. The rice husk was quickly burnout, so the flame was unstable and discontinuous. Thus, the smoldering spread was dominant in Stage I.

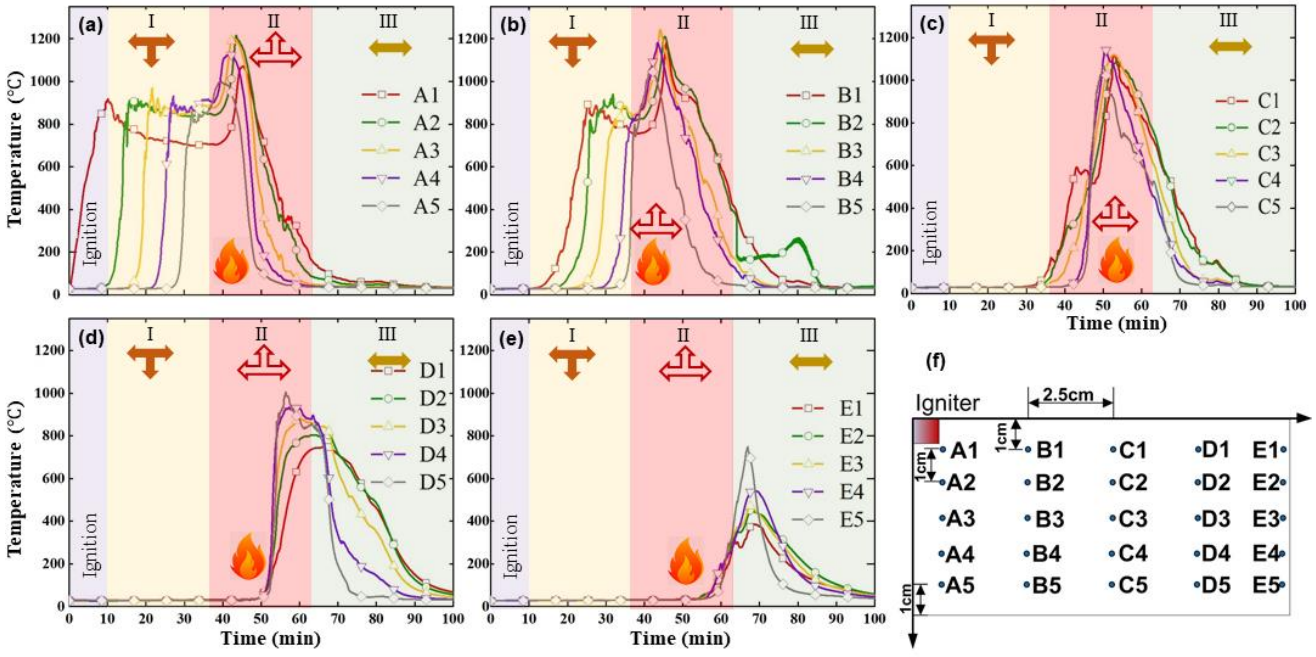

Fig. 6. Temperature inside the rice sample during the ignition and fire spread under a forced drying airflow of 0.6 m/s, (a) 0 cm, (b) 2.5 cm, (c) 5 cm, (d) 7.5 cm, and (e) 10 cm from the central axis, and (f) locations of all thermocouples, where the arrow shows the dominating fire spread directions during different stages, the solid arrow shows the smoldering spread, and the hollow arrow shows the flame spread.

The smoldering peak temperature of rice was 800-900 °C (Fig. 6a-b and Fig. 7a), which was much higher than smoldering fires in peat [36] and cotton [37], but comparable to coal fire [29, 38]. As the temperature of smoldering rice particles was comparable to the rod igniter, it was hot enough to emit visible light (i.e., the glowing phenomenon [30, 32]), even if there was no flame inside the porous rice bed at this stage. The smoldering spread is a volumetric process [30], so it spreads both horizontally and downward into the rice sample. For the convective drying process, the primary oxygen supply for the smoldering spread was from the forced drying airflow.

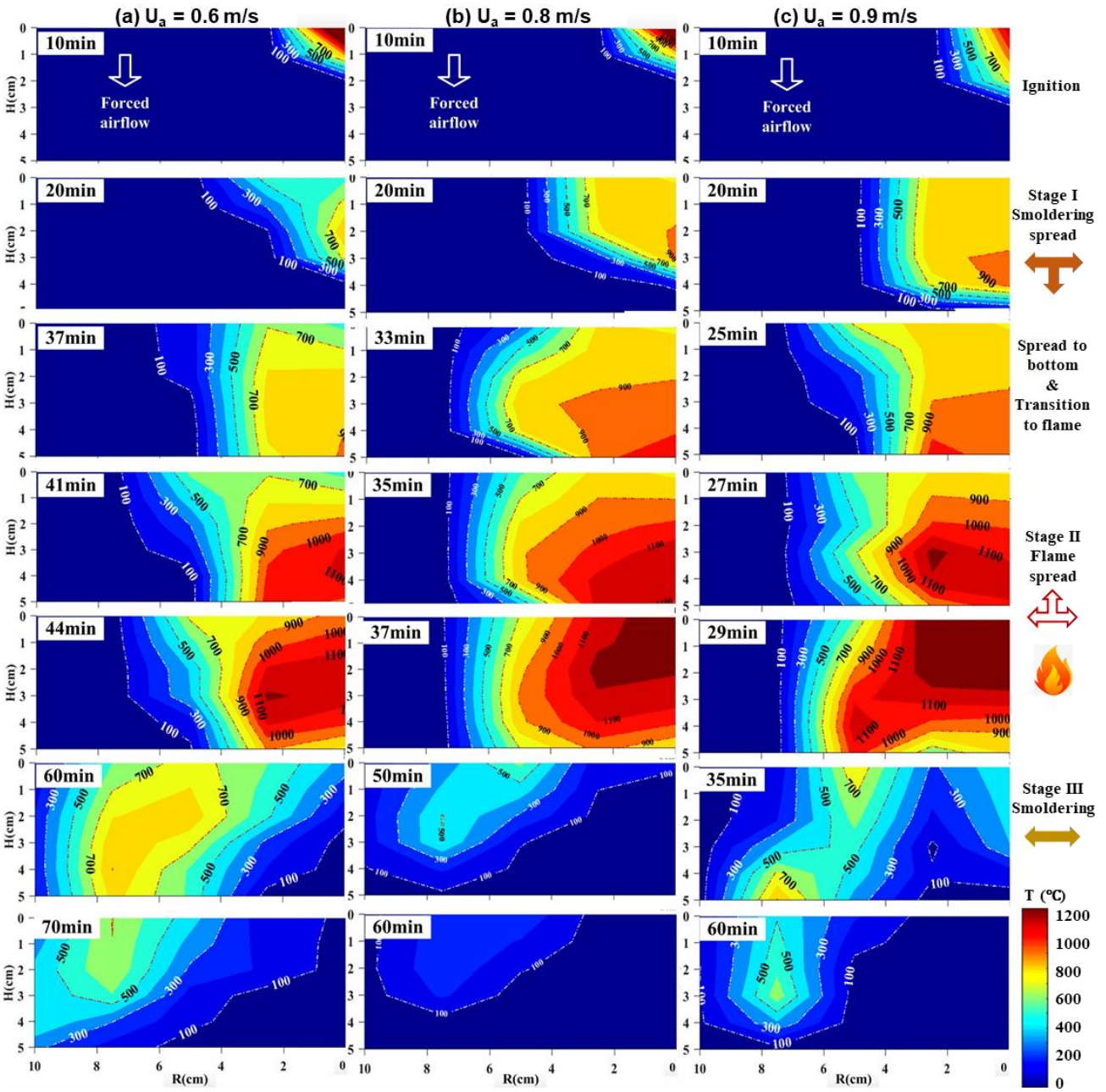

Fig. 7. Reconstructed temperature contour inside the rice bed under the forced drying airflow of (a) 0.6 m/s (Video S5), (b) 0.8 m/s (Video S6), and (c) 0.9 m/s (Video S7), where the arrow shows the dominating fire spread directions during different stages, the solid arrow shows the smoldering spread, and the hollow arrow shows the flame spread.

At the airflow velocity of 0.6 m/s, the horizontal and downward spread rates are comparable, as shown by the fire-spread processes in Fig. 7a. Specifically, after about 30 min, the smoldering front reached the bottom free surface that was 5 cm below the top, and the horizontal spread distance was also about 5 cm. Note that with the internal airflow, the internal horizontal smoldering spread could be comparable to free-surface horizontal spread, which is different from most natural smoldering fires without the internal airflow. Without the internal airflow, the free surface has the best oxygen supply; thus, the smoldering spread near the free

surface will be much faster than the internal (or in-depth) spread, such as in peat [36, 39] and cotton [37].

Moreover, because both the internal airflow and smoldering spread were in the downward direction, the downward spread was a concurrent spread. The concurrent smoldering spread is essentially a burning or fuel regression process [32, 35], so the rice beneath the charred top surface was burnout to create a cavity (see Fig. 8). The rice layer on the top surface did not collapse because (1) the pyrolysis of rice also produced sticky tars to hold rice particles, and (2) the thermocouple matrix helped to hold the top residue shell. Figure 7b-c further shows the temperature contour inside the rice bed based on thermocouple temperature measurements under the airflow velocities of 0.8 and 0.9 m/s, respectively. Essentially, as the airflow velocity increases, the downward smoldering spread inside the rice sample increases (see more discussions in Section 3.3).

Stage-II Flame Spread. Afterward, the smoldering-to-flaming (StF) transition occurred on the sample bottom surface at about 37 min, which initiated the flaming Stage II**.** There were three causes for this StF transition, (1) the burnout of rice bed significantly reduced the flow resistance and increased airflow velocity, (2) the volume of the smoldering region was increased, where sufficient flammable pyrolysis gases were produced, and (3) Stage-I smoldering (glowing) surface was hot enough (>800 °C) to pilot flammable mixture.

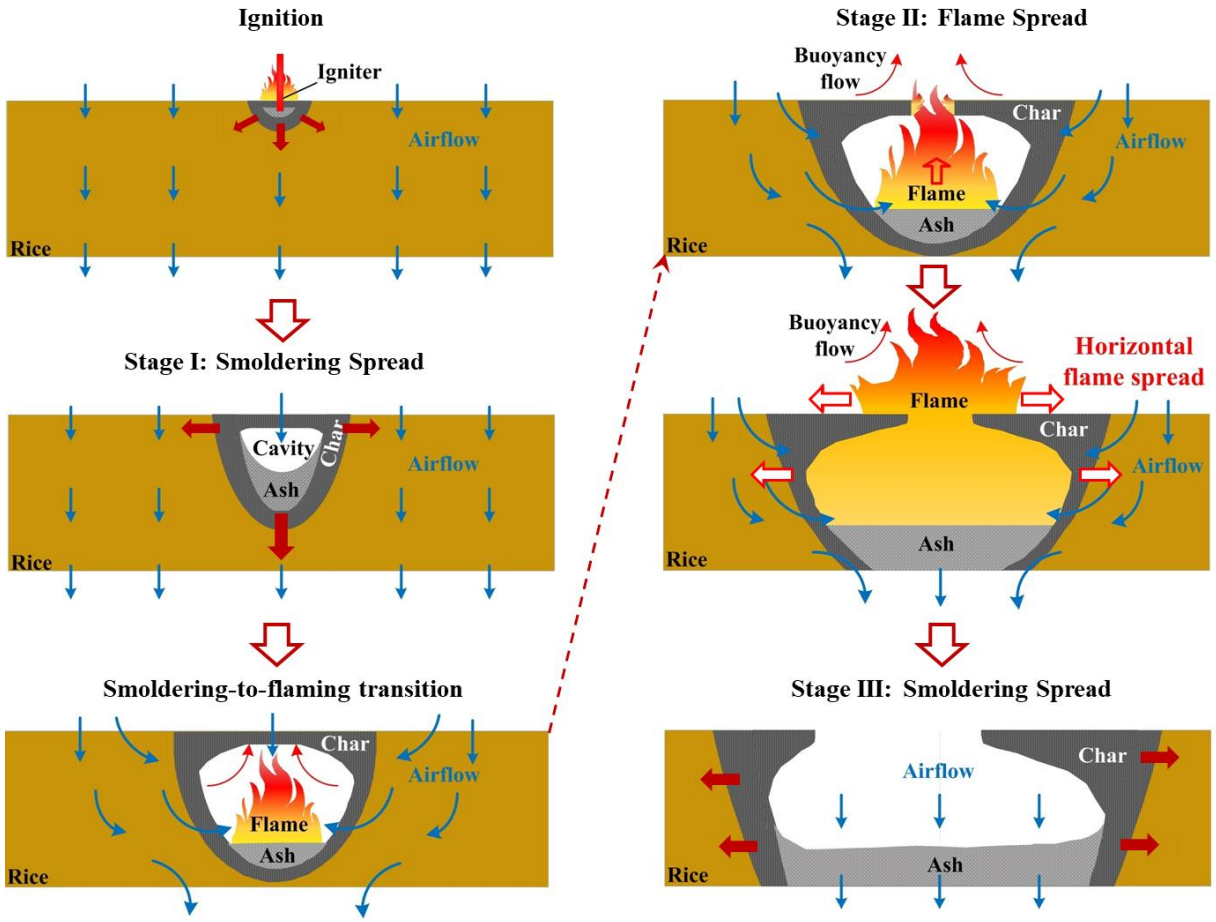

Fig. 8. The schematic diagram of the three-stage fire spread and the regression of the rice bed in the drying chamber.

As the Stage-II flame spread was beneath the top surface, it was challenging to observe the flame visually (see Fig. 5 and Video S2). Nevertheless, the glowing region on the top surface was found to gradually increase, as it was heated by the flame tip below. Moreover, the internal temperature increased rapidly to above 1100 °C (see Fig. 6a-b and Fig. 7a), indicating the existence of flame. The flame grew quickly and, eventually, reached and ignited the top surface. Thus, the duration of upward flame spread was short, where the flame above the top surface occurred only a few minutes after the StF transition.

At the same time, the flame spread horizontally on the rice bed below the top charred shell (see the hot cavity in Fig. 7 and the illustration in Fig. 8). The flame exceeded the top surface and became taller at a larger airflow. Thus, the flame seems to "spread" horizontally on the top surface as well, and such a spread was initially in the radial direction, but quickly became random, showing a finger-like pattern [32, 40]. These behaviors were quite deceptive and could hide the actual flame spread below. Especially when the airflow was

small, it was difficult to observe the strong internal flame spread from the top view. Nevertheless, the scrutiny could still reveal the difference from a typical flame spread on the fuel surface. The surface rice particles within the flame were glowing (Fig. 5 and Videos 2-4) and much hotter than the charring temperature (about 400 °C in Fig. A1), which indicated that they were heated by the flame below rather than that a flame was maintained above the top surface.

The actual horizontal flame spread beneath the free surface could be quantified by the thermocouple matrix (Fig. 7). As expected, the flame spread was much faster than the smoldering spread, so the burning area (see hot spots inside the rice bed in Fig. 7 and Videos S5-7) quickly expanded and reached the chamber wall within 10 min. At the same time, the mass-loss rate quickly increased to a peak (see Fig. 4b). After flame spread over, thermocouples started to measure the temperature of rice residue and smoke, so the temperature quickly decreased below 500 °C.

Stage-III Horizontal Smoldering Spread. After about 60 min, the flame on rice gradually weakened as the flame front reached the chamber wall, and eventually transition back to smoldering. The extinction of flame was because all rice particles had been pyrolyzed into char, and there was no pyrolysis gas to support the flame. The smoldering fire front continued to spread horizontally over the remaining char, which lasted for another 40-60 min before the true extinction. Such a long-lasting smoldering end-stage can also be a significant fire hazard, which is able to trigger another transition to flame with the feed of fresh rice and release a significant amount of toxic gases [30, 41]. Due to the cooling from the cold wall, the smoldering peak temperature was about 700 °C (see Fig. 6d-e and Fig. 7a), which was much lower than Stage I (800-900 °C). Eventually, the smoldering on charred rice was quenched near the wall [34] before burnout.

3.3 Fire spread rate and effect of drying airflow

Figure 7 further compares the influence of the drying airflow on the temperature and smoldering spread pattern of the burning rice. As seen from the motion of the hot region in the smoldering Stage-I, the downward spread rate increased with the velocity of internal airflow, and it eventually exceeded the horizontal spread. For the horizontal spread, the spread profile was uniform with the depth, where the overhang structure [36] did not appear, because the forced airflow provided an excellent oxygen supply in-depth. To further reveal if the Stage-I smoldering spread was accelerating or steady-state, the spatial variation of smoldering spread rate was calculated by the tracking the arrival of smoldering (or char-oxidation) front. Based on thermal analysis data (Fig. A1), the thermocouple temperature of 400 °C was used to identify the smoldering front, and a MATLAB code was programmed to conduct the calculation.

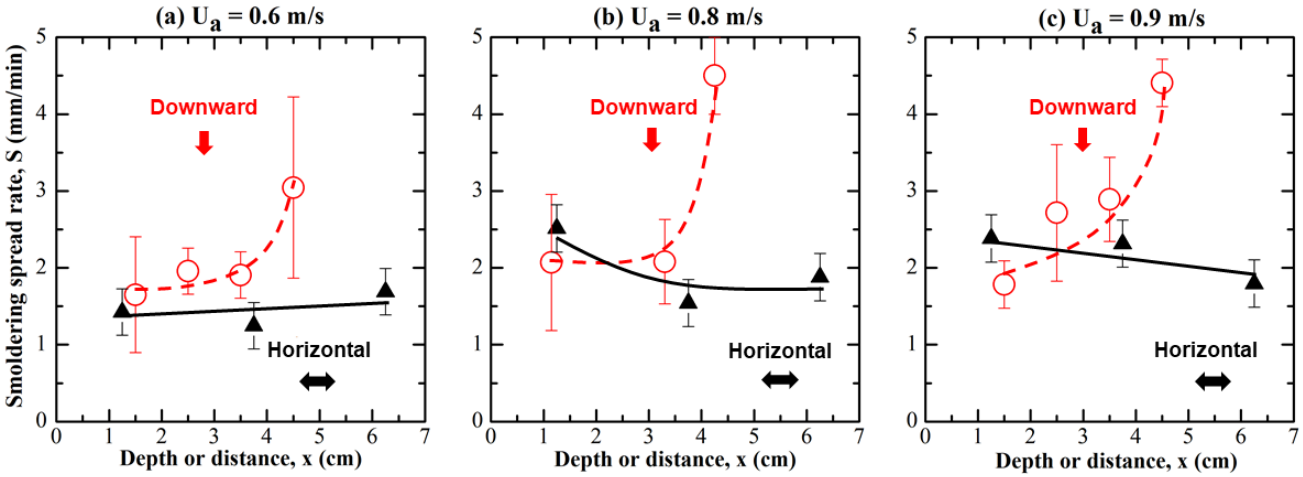

Fig. 9. Stage-I downward and horizontal smoldering spread rate vs. depth under the drying airflow velocities of (a) 0.6 m/s, (b) 0.8 m/s, and (c) 0.9 m/s, where the error bars showed the uncertainty in all repeating tests.

The concurrent smoldering spread rate (S) is essentially the burning regression rate ($\dot{R}$) [30, 32] that is controlled by the oxygen supply as

$$S = \dot{R} = \frac{\dot{m}''_F}{\rho_F} = \frac{\dot{m}''_{O_2}}{\gamma_{O_2}\rho_F} = \frac{\rho_a Y_{O_2}}{\gamma_{O_2}\rho_F} U_a \tag{3}$$

where $\dot{m}''_F$ is the fuel burning flux, $\dot{m}''_{O_2} = Y_{O_2}\rho_a U_a$ is the mass flux of oxygen supply, and γ_{O_2} is the stoichiometric coefficient for oxygen. Figure 9 summarizes the Stage-I downward spread rate vs. the depth and the horizontal spread rate vs. the radial distance. It is apparent that the downward (concurrent) smoldering spread rate increases with the depth, especially when it approaches the bottom. Specifically, the spread rate increases from about 2 mm/min near the top surface to about 4 mm/min near the bottom surface. It is because the burnout of rice layer reduces the flow resistance and increases the internal airflow velocity (U_a) under the constant extraction power.

On the other hand, the horizontal smoldering spread was mostly steady-state. Specifically, the horizontal smoldering spread rate over rice was 2 ± 0.5 mm/min, which was close to peat [36] and cotton [37]. Note that the horizontal spread rate was comparable to or smaller than the downward spread, the trend of which was opposite to the natural smoldering fire without forced internal flow. For the natural smoldering fire (like the peat fire), there is no forced airflow inside the porous fuel, and the oxygen supply is controlled by diffusion within the surface boundary layer. Thus, the oxygen supply for the horizontal spread is maximum, but decreases with the increasing depth for the vertical (downward or upward) spread [35, 38].

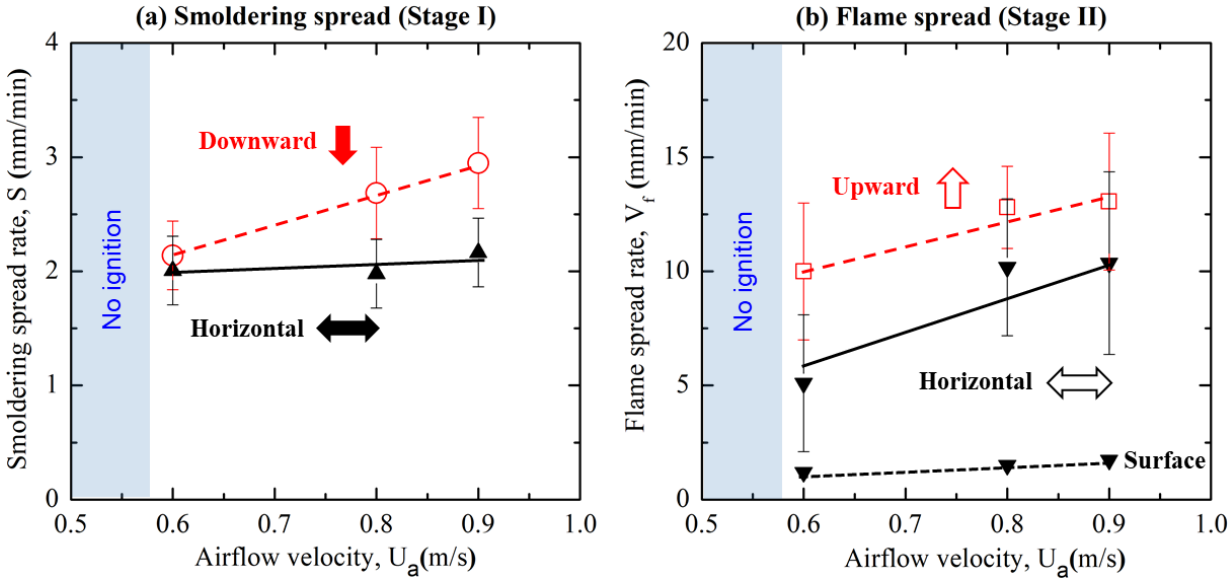

Fig. 10. Effect of drying airflow velocity on fire spread rate, (a) Stage-I downward and horizontal smoldering spread, and (b) Stage-II upward and horizontal flame spread.

Figure 10 quantified the effect of drying flow velocity on the fire spread rate, (a) the Stage-I smoldering spread, and (b) the Stage-II flame spread. For the downward smoldering spread (Fig. 10a), the spread rate increased almost linearly with the downward drying airflow, as explained by Eq. (3). On the other hand, the horizontal smoldering spread rate remained at 2 mm/min and, as expected, was insensitive to the downward drying airflow. The rate of Stage-II flame spread (about 10 mm/min) was much larger than that of Stage-I smoldering spread (about 2 mm/min).

Figure 10b also shows that the upward flame spread is faster than then horizontal spread. Moreover, flame-spread rates in both directions increased almost linearly with the drying airflow. On the other hand, the trend of horizontal flame spread was different from the unchanged horizontal smoldering spread rate. It is because the flame spread in both directions is controlled by the convection that always increases with the airflow. As discussed above, the horizontal flame spread occurred below the top surface (see Fig. 8), and the flame was taller than the top surface. Thus, visually the flame seemed to "spread" on the top surface as well (see Fig. 5 and Videos S2-4). As also plotted in Fig. 10b, such a flame motion was extremely slow (about 1 mm/min), which was even slower than the smoldering spread. This deceptive slow flame motion on the top surface hides the fast flame-spread behaviors below, which can cause an underestimation of the fire development and hazard. Thus, it is critical to monitor the internal temperature of rice and other grains during the convective drying process, in order to discover the smoldering hot spot, identify the real motion of flame, and determine the actual extinction moment.

4. Conclusions

This work investigated the ignition risk and fire behavior of bench-scale paddy rice (about 1 kg and 2 L) in the convective drying process with an internal airflow velocity up to 0.9 m/s. Results showed that there was a minimum internal airflow velocity for given spotting ignition protocol, simulated by a glowing rod. A larger drying airflow showed a greater ignition risk.

Once ignited, three stages of hidden fire spread processes below the surface were revealed, (I) smoldering spread, (II) flame spread, and (III) smoldering spread. The smoldering rice was glowing hot and had a peak temperature between 800 °C and 900 °C. With a large forced internal airflow, the downward smoldering spread (about 2 mm/min) was comparable to or faster than the horizontal spread, different from the natural smoldering fire. The regression of rice bed in Stage-I smoldering increased the drying airflow, which not only accelerated the downward smoldering spread with depth, but also triggered the smoldering-to-flaming transition and a flame spread. The Stage-II flame mainly spread beneath the top surface, which was difficult to identify. After flame extinction, the Stage-III smoldering could continue to burn for an extensive period. By increasing the drying airflow velocity, the fire-spread rate in all stages increased, and the burnout time decreased, indicating a more significant fire hazard.

It is also recommended to monitor the internal temperature of the rice and other grains during the convective drying process, in order to discover the smoldering hot spot, identify the hidden motion of flame below the fuel surface, and determine the actual extinction moment. This work reveals the complex smoldering and flaming fire dynamics of rice and provides scientific support for fire protection during the grain drying process.

Acknowledgments

This work was supported by the National Key R&D Program of China (2017YFC0805900), National Natural Science Foundation of China (NSFC) No. 51876183, the Fundamental Research Funds for the Central Universities (WK2320000041, WK2320000043), and State Key Laboratory of Fire Science Open Fund (No. HZ2019-KF02).

References

[1] M.A. Bashir, J. Liu, Y. Geng, H. Wang, J. Pan, D. Zhang, A. Rehim, M. Aon, H. Liu, Co-culture of rice and aquatic animals: An integrated system to achieve production and environmental sustainability, Journal of Cleaner Production, (2019) 119310.

[2] W. Sha, F. Chen, A.K. Mishra, Adoption of direct seeded rice, land use and enterprise income: Evidence from Chinese rice producers, Land Use Policy, 83 (2019) 564-570.

[3] L. Amagliani, J. O'Regan, A.L. Kelly, J.A. O'Mahony, The composition, extraction, functionality and applications of rice proteins: A review, Trends in Food Science & Technology, 64 (2017) 1-12.

[4] I. Quispe, R. Navia, R. Kahhat, Energy potential from rice husk through direct combustion and fast pyrolysis: A review, Waste Manag, 59 (2017) 200-210.

[5] P. Unrean, B.C. Lai Fui, E. Rianawati, M. Acda, Comparative techno-economic assessment and environmental impacts of rice husk-to-fuel conversion technologies, Energy, 151 (2018) 581-593.

[6] P. Girardon, Safety Improvement by Means of Gas Applications; Fire Prevention in Frozen Food Storages and Grain Silos, in: Gases in Agro-Food Processes, Academic Press, 2019, pp. 585-588.

[7] A. Ramirez, J. Garcia-Torrent, P.J. Aguado, Determination of parameters used to prevent ignition of stored materials and to protect against explosions in food industries, J Hazard Mater, 168 (2009) 115-120.

[8] A. Ramirez, J. Garcia-Torrent, A. Tascon, Experimental determination of self-heating and self-ignition risks associated with the dusts of agricultural materials commonly stored in silos, J Hazard Mater, 175 (2010) 920-927.

[9] M. Abuswer, P. Amyotte, F. Khan, S. Imtiaz, Retrospective risk analysis and controls for Semabla grain storage hybrid mixture explosion, Process Safety and Environmental Protection, 100 (2016) 49-64.

[10] X. Ma, J. Hu, X. Wang, S. Choi, T.-A. Zhang, Y.F. Tsang, M.-T. Gao, An integrated strategy for the utilization of rice straw: Production of plant growth promoter followed by ethanol fermentation, Process Safety and Environmental Protection, 129 (2019) 1-7.

[11] S. Shafiekhani, S.A. Wilson, G.G. Atungulu, Impacts of storage temperature and rice moisture content on

color characteristics of rice from fields with different disease management practices, Journal of Stored Products Research, 78 (2018) 89-97.
[12] L. Su, B.D. Adam, F.H. Arthur, J.L. Lusk, J.F. Meullenet, The economic effects of Rhyzopertha dominica on rice quality: Objective and subjective measures, Journal of Stored Products Research, 84 (2019) 101505.
[13] I. Ahmad, A. Noomhorm, Grain Process Engineering, Asian Institute of Technology, Khlong Nueng, Thailand, 2019.
[14] F. Fleurat-Lessard, Postharvest Operations for Quality Preservation of Stored Grain, Materials Science, (2016) 117-125.
[15] K.J. Hellevang, Grain Drying, North Dakota State University, Fargo, North Dakota, 2013.
[16] S. Heidenreich, M. Müller, P.U. Foscolo, Chapter 3 - Biomass Pretreatment, in: S. Heidenreich, M. Müller, P.U. Foscolo (Eds.) Advanced Biomass Gasification, Academic Press, 2016, pp. 11-17.
[17] Z.M. Gitonga, H. De Groote, M. Kassie, T. Tefera, Impact of metal silos on households' maize storage, storage losses and food security: An application of a propensity score matching, Food Policy, 43 (2013) 44-55.
[18] Y. Pan, H. Fang, B. Li, F. Wang, Stability analysis and full-scale test of a new recyclable supporting structure for underground ecological granaries, Engineering Structures, 192 (2019) 205-219.
[19] V. Babrauskas, Ignition Handbook, Fire Science Publishers/Society of Fire Protection Engineers, Issaquah, WA, 2003.
[20] L. Ding, F. Khan, J. Ji, Risk-based safety measure allocation to prevent and mitigate storage fire hazards, Process Safety and Environmental Protection, 135 (2020) 282-293.
[21] M. Christopherson, Fire at Cenex Harvest States grain dryer, in, 2009. https://www.crookstontimes.com/article/20091019/NEWS/310199969
[22] C. Newsroom, Crews battle accidental grain dryer fire in Mount Pleasant, in, 2018. https://www.cbs58.com/news/fire-reported-at-county-kr-and-100th-in-mount-pleasant
[23] A. Rolheiser, Feed barley lost in early morning grain dryer fire, in, 2019. https://farmnewsnow.com/2019/10/01/feed-barley-lost-in-early-morning-grain-dryer-fire/
[24] R.F. de Lima, R.G. Dionello, C. Peralba Mdo, S. Barrionuevo, L.L. Radunz, F.W. Reichert Junior, PAHs in corn grains submitted to drying with firewood, Food Chem, 215 (2017) 165-170.
[25] A.C. Fernandez-Pello, Wildland fire spot ignition by sparks and firebrands, Fire Safety Journal, 91 (2017) 2-10.
[26] S. Wang, X. Huang, H. Chen, N. Liu, Interaction between flaming and smouldering in hot-particle ignition of forest fuels and effects of moisture and wind, International Journal of Wildland Fire, 26 (2017) 71-81.
[27] X. Huang, G. Rein, Thermochemical conversion of biomass in smouldering combustion across scales: The roles of heterogeneous kinetics, oxygen and transport phenomena, Bioresource Technology, 207 (2016) 409-421.
[28] S. Lin, P. Sun, X. Huang, Can peat soil support a flaming wildfire?, International Journal of Wildland Fire, 28 (2019) 601-613.
[29] Z. Song, X. Huang, r.C. Kuenze, H. Zhu, J. Jiang, X. Pan, X. Zhong, Chimney effect induced by smoldering fire in a U-shaped porous channel: A governing mechanism of the persistent underground coal fires, Process Safety and Environmental Protection, 136 (2020) 136-147.
[30] G. Rein, Smoldering Combustion, SFPE Handbook of Fire Protection Engineering, 2014 (2014) 581-603.
[31] M.A. Santoso, E.G. Christensen, J. Yang, G. Rein, Review of the Transition From Smouldering to Flaming Combustion in Wildfires, Frontiers in Mechanical Engineering, 5 (2019).
[32] X. Huang, J. Gao, A Review of Near-Limit Opposed Fire Spread, Fire Safety Journal, (2020).
[33] K.R. Bhattacharya, C.M. Sowbhagya, Y.M.I. Swamy, Some physical properties of paddy and rice and their interrelations, Journal of the Science of Food and Agriculture, 23 (1972) 171-186.
[34] S. Lin, X. Huang, Quenching of Smoldering: Effect of Wall Cooling on Extinction, Proceedings of the Combustion Institute (under review), (2020).
[35] X. Huang, G. Rein, Upward-and-downward spread of smoldering peat fire, Proceedings of the Combustion Institute, 37 (2019) 4025-4033.

[36] X. Huang, F. Restuccia, M. Gramola, G. Rein, Experimental study of the formation and collapse of an overhang in the lateral spread of smouldering peat fires, Combustion and Flame, 168 (2016) 393-402.
[37] Q. Xie, Z. Zhang, S. Lin, Y. Qu, X. Huang, Smoldering of high-density cotton bale under concurrent wind, Fire Technology, (2020) in press.
[38] F. He, F. Behrendt, Experimental investigation of natural smoldering of char granules in a packed bed, Fire Safety Journal, 46 (2011) 406-413.
[39] E.G. Christensen, N. Fernandez-anez, G. Rein, Influence of soi l conditions on the multidimensional spread of smouldering combustion in shallow layers, 214 (2020) 361-370.
[40] S.L. Olson, F.J. Miller, S. Jahangirian, I.S. Wichman, Flame spread over thin fuels in actual and simulated microgravity conditions, Combustion and Flame, 156 (2009) 1214-1226.
[41] Y. Hu, N. Fernandez-Anez, T.E.L. Smith, G. Rein, Review of emissions from smouldering peat fires and their contribution to regional haze episodes, International Journal of Wildland Fire, 27 (2018) 293-312.

Appendix

The thermal analysis (both TGA and DSC) was conducted with a PerkinElmer STA 6000 Simultaneous Thermal Analyzer. Before analysis, the rice sample was first pulverized and then dried at 105 ℃ for 20 min. The initial mass of cotton was about 10 mg, and sample was heated at a constant rate, and six heating rates, 5, 10, 15, 20, 30, and 40 K/min were tested. The test environment was airflow with a flow rate of 50 mL/min. Each condition was tested twice to ensure the experimental repeatability. Figure A1 shows the mass-loss rate and heat flow curves of this rice sample at the heating rate of 5 K/min and 40 K/min. As the heating rate in the bench-scale rice fire is comparable or higher than 40 K/min, the thermal-analysis data with a higher heating is more relevant. As indicated by the fast increase of mass-loss rate and heat-release rate, the decomposition of rice starts at about 300 ℃, and the second-stage char oxidation starts at about 400 ℃. The heat of smoldering for rice can be calculated by integrating the heat flow curve, and it is about 8 MJ/kg, which is lower than that of peat [28] and cotton [37].

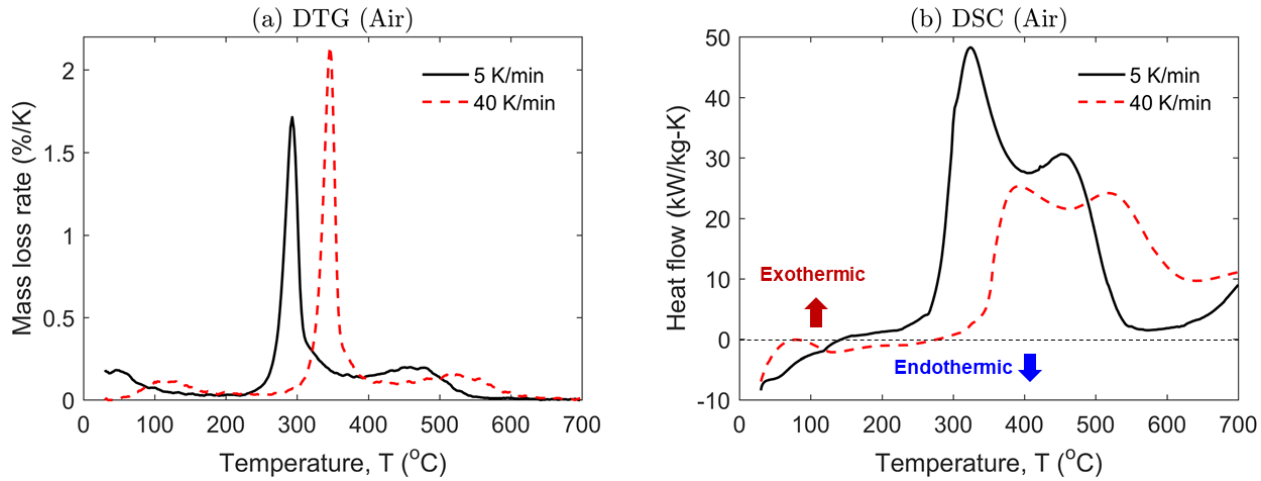

Fig. A1. (a) Mass-loss rate (DTG), and (b) heat flow (DSC) curves of rice in air atmosphere with the heating rates of 5 and 40 K/min.